RSC Advances

PAPER

View Article Online
View Journal | View Issue

Cite this: *RSC Adv.*, 2017, **7**, 14709

Structure and crystallization behavior of Al containing glasses in the $CaO–B_2O_3–SiO_2$ system

Jiao Han,*[a] Yuanming Lai,[b] Yao Xiang,[a] Shuang Wu,[a] Yiming Zeng,*[a] Hongwei Yang,[a] Yongyun Mao[a] and Yuwen Yang[a]

Received 4th February 2017
Accepted 27th February 2017

DOI: 10.1039/c7ra01427a

rsc.li/rsc-advances

The aim of the present work is to investigate the effects of Al_2O_3 content on both the structure and crystallization behavior of $CaO–B_2O_3–SiO_2$ (CBS) glass composition using NMR, FT-IR and DSC. The density experimental results showed that the density (ρ) of glasses decreased linearly with increasing Al_2O_3 content, while the molar volume (V_m) of the glasses increased linearly. The NMR revealed that the Al occurred in the forms of Al^{IV}, Al^{V} and Al^{VI} units. With the increasing Al_2O_3 content, the amount of Al species show little change, the relative amount of B^{IIIa} and B^{IIIs} units increases while the B^{IV} units decrease, and the Q^4 structural units increases clearly but the Q^3 decreases. Further, crystallization peaks of CBS glasses shift to higher temperatures, indicating that Al_2O_3 addition can suppress crystallization of CBS glasses.

1. Introduction

During the second half of the 19th century, borosilicate optical glass was first studied to offer systematic insight into the relationships between the composition of glass and its physical and chemical properties. After this, $CaO–B_2O_3–SiO_2$ (CBS) glasses have been a popular study point over the years due to their excellent properties in a number of fields, for instance, high emissivity coating materials,[1] optical glasses for smart window applications,[2] or as bioactive materials to prevent microfouling,[3] or also as storage materials for dealing with nuclear waste[4] and electronic glasses in low temperature co-fired ceramics (LTCC) technology.[5]

In order to satisfy the need of the technical applications in different fields, the optimization in glasses is carried out in composition and structure of the glasses to achieve the required physical, mechanical and dielectric properties. Introduction of intermediate oxides, such as ZnO,[3,6] ZrO_2 (ref. 7) and Al_2O_3,[8] in borosilicate glass can be an effective way to change structure of glass. They can act either as glass modifier or glass former, depending upon their amount in glass composition. The oxide addition in glass system will lead to the change of NBOs, resulting in the formation of different structural units within the glass network. This will make great contribution optimize the chemical, thermal stability and various properties (physical properties and dielectric properties) of glasses. Colak *et al.*[6] reported the dramatic effect (modifier or network former) of ZnO in borate glass structure due to the non-bridging oxygen atoms. The ZnO played as a network former when having more than 5% (weight%) ZnO in glasses, on the contrary, the role was modifier. Khan *et al.*[7] did some research about the modification in yttrium calcium borosilicate glasses units by ZrO_2 instead of CaO. Interestingly higher content of ZrO_2 ≥7.5 mol% may be acts as glass former and below 7.5 mol%, it may act as glass modifier. Also, the variation in structure leads to the change of optical and dielectric properties. Neuville *et al.*[9] found that Al/Si tetrahedral distribution in the glass network in different Q^n units depending on the join R=CaO/Al_2O_3. The results revealed the remarkable function of aluminum in $CaO–Al_2O_3–SiO_2$ (CAS) ternary glass system. Aluminoborosilicate glasses consist of structural units, such as BO_3, BO_4,[10] SiO_4,[11] AlO_4 and AlO_6 (ref. 12) species. The transformation of network formers in aluminosilicate glasses can make the structure of $CaO–B_2O_3–SiO_2$ glass meet the application need.

However, so far, there is no report about utilizing FT-IR spectra, NMR, DSC and XRD to research the structure and crystallization of calcium aluminoborosilicate glasses with varying Al content. Therefore, in this paper, we present a detailed report on the structure and crystallization of $CaO–B_2O_3–SiO_2$ glass with Al_2O_3 content, especially the relationship between the Al content and the impacts on the units of glass network, which will provide guiding significance for further optimization of the glass structure.

2. Experimental

2.1 Preparation of glass samples

The $(1 - x/100) \times (35CaO–37SiO_2–28B_2O_3) + xAl_2O_3$, where x = 0, 1, 2.5, 5, 7.5 and 10 mol%, were prepared using analytically

[a]State Key Laboratory of Advanced Technologies for Comprehensive Utilization of Platinum Metals, Kunming Institute of Precious Metals, Kunming 650106, PR China. E-mail: hanjiao90@sina.com; zengym0871@126.com
[b]State Key Laboratory of Electronic Thin Films and Integrated Devices, University of Electronic Science and Technology of China, Chengdu 610054, PR China

pure $CaCO_3$, H_3BO_3, SiO_2, and Al_2O_3 as the starting materials. The stoichiometric amounts of chemicals were mixed homogeneously and transferred to Pt crucibles to melt at a temperature of 1400 °C for 2 h in air. After melting, the melt was quickly quenched into deionized water and ground, followed by screened through a 500-mesh stainless steel wire screen to obtain glass powders with particle size less than 25 μm.

2.2 Characterization of the samples

The XRD patterns of crushed powder samples were recorded within angular range 10–80° using PANalytical X'Pert PRO with Cu Kα radiation ($\lambda = 1.54$ Å). The 2θ angle scans were made at step width of 0.02° and a time per step of 0.5 s.

The density of all glasses was examined using AccuPyc®II 1340 (Micromeritics USA). The data was tested ten times to obtain an accurate density value. Fourier transform infrared spectra (FT-IR, Thermo Nicolet Smart-380) were carried out in the range 400–2000 cm^{-1} at room temperature with a resolution of 2 cm^{-1} on glass powders. Samples were mixed with spectroscopic grade dry KBr powder and then compressed the mixtures to obtain pellets for FT-IR measurements.

A Differential Scanning Calorimetry (DSC, STA409 PG/PC, Netzsch, Germany) was carried out to determine the glass transition temperature (T_g) and the crystallization behavior. The test was conducted in a flowing atmosphere of dry air from ambient temperature to 1000 °C with a heating rate of $\beta = 5$ °C min^{-1}. The DSC experiments were carried out using alumina crucibles with a-Al_2O_3 powder as a reference material.

^{11}B, ^{27}Al and ^{29}Si magic angle spinning nuclear magnetic resonance spectroscopy (MAS-NMR, Varian Infinity-plus 400) were performed on all glasses to determine the roles of B, Si and Al in glasses system. The definite test condition refers to ref. 13.

3. Results and discussion

3.1 The XRD analysis

Fig. 1 presented the X-ray diffraction conducted on the glasses, which showed the diffusion peaks and no crystalline phases, indicating the amorphous state of all glasses.

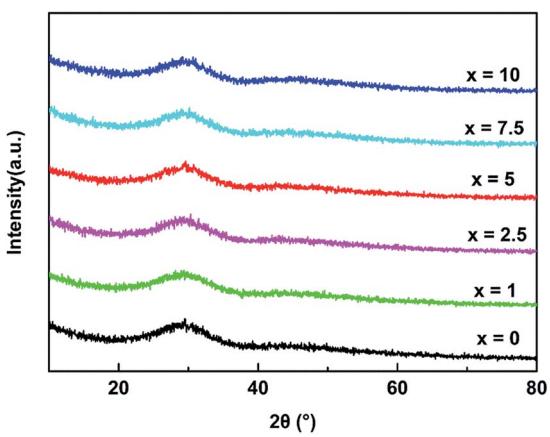

Fig. 1 X-ray diffraction patterns of glasses.

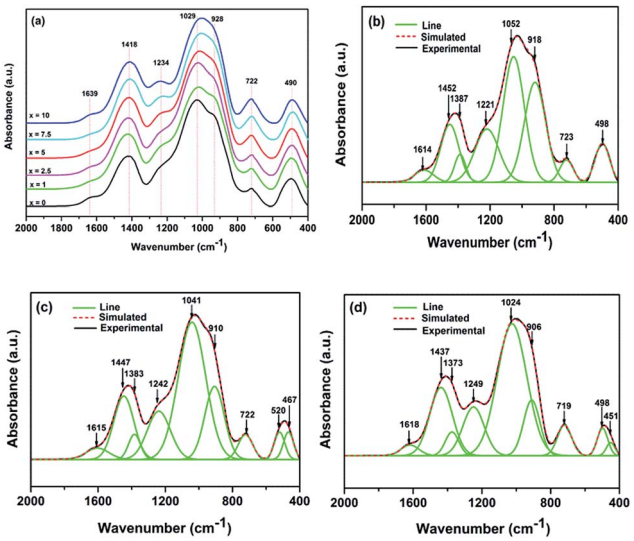

Fig. 2 (a) The FT-IR spectra of the glasses; deconvoluted FT-IR spectra of the glasses based on Gaussian function, (b) $x = 0$, (c) $x = 5$, (d) $x = 10$.

3.2 The FT-IR analysis

The FT-IR spectra of all glasses for $x = 0$, 1, 2.5, 5, 7.5 and 10 mol% between 400 and 2000 cm^{-1} are shown in Fig. 2(a), respectively. The broad bands showed in FT-IR absorbance spectra confirm the amorphous nature (as showed in Fig. 1) and wide distribution of Q^n (Q^n notation indicates n bridging oxygen per tetrahedron) units of glasses. All experimental glass compositions showed similar FT-IR spectra and the absorption bands are broad resulting in different component peaks to form overlap easily. Therefore, it is necessary to utilize the deconvolution based on Gaussian function to identify each component peak of all bands in the FT-IR spectra to realize their assignments. Fig. 2(b)–(d) represent the deconvoluted spectra of glasses for $x = 0$, $x = 5$ and $x = 10$ mol% as examples of the glasses investigated, respectively. The high frequency band around 1620 cm^{-1} is attributed to the molecular water.[14] The band near 1450 cm^{-1} and 1380 cm^{-1} are characteristic of antisymmetric stretching vibration of $[BO_3]$.[15] The band at 1234 cm^{-1} is due to the corresponding mode of borate triangles with non-bridging oxygen (NBO) atoms, which are mainly BO_2O^- triangles with two bridging and one non-bridging oxygen atom.[16] It is notable that the intensity of the band at 1234 cm^{-1}

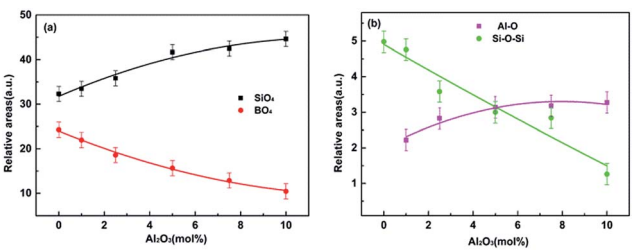

Fig. 3 Dependence of the relative area of SiO_4, BO_4 group (a) and Al–O, Si–O–Si (b) on Al_2O_3 content. The lines are guide for the eyes.

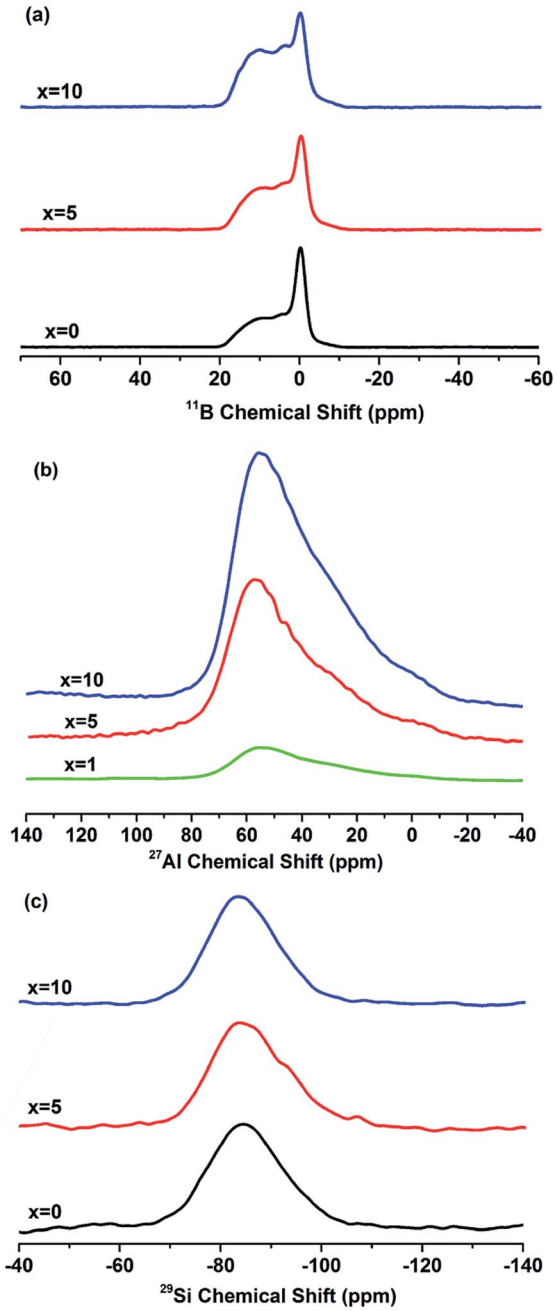

Fig. 4 NMR spectra of (a) ^{11}B, (b) ^{27}Al and (c) ^{29}Si of experimental glasses.

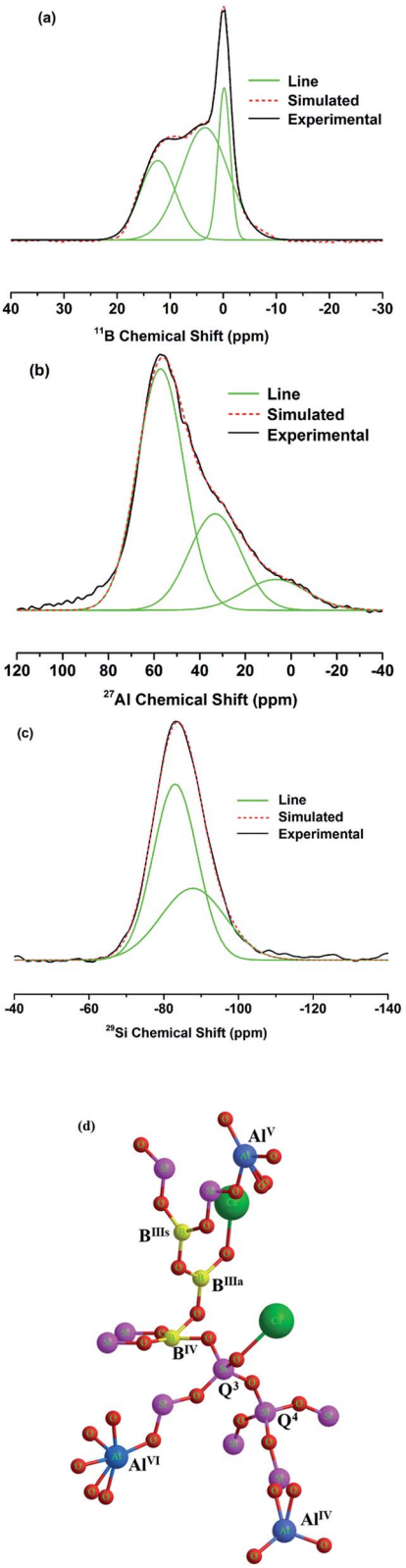

Fig. 5 Deconvolution of (a) ^{11}B, (b) ^{27}Al and (c) ^{29}Si NMR spectra for glass with $x = 5$. (d) The ball-and-stick models for species in glasses.

increases gradually with the Al_2O_3 content increasing, revealing the enhancement of borate triangles with NBOs proportion in glasses. The band located around 1030 cm^{-1} assigned to the merging bands of the SiO_4 tetrahedral,[4] and the band shifted to lower wavenumber, the wavenumber of this band location are separately 1052, 1048, 1043, 1041, 1036, 1024 cm^{-1} from $x = 0$ to $x = 10$, respectively, indicating the addition of Al_2O_3 may change the combination mode in glasses. The band near 910 cm^{-1} is due to B–O stretching in BO_4 units[17] and its intensity becomes weaker as the increasing Al_2O_3 content. Additionally, the relative areas of the peak corresponding to SiO_4 and BO_4 units were calculated according to the assignment of the IR spectra, showed in Fig. 3(a). It reveals that the amount of SiO_4 increase while the BO_4 units reduce in glass system with the

Table 1 NMR parameters for ^{11}B deconvolution

	Boron site	δ_{iso} (ppm)	Amount (%)
$x = 0$	B^{IIIa}	11.97	26.44
	B^{IIIs}	3.17	44.68
	B^{IV}(1B,3Si)	−0.28	28.88
$x = 5$	B^{IIIa}	12.33	28.14
	B^{IIIs}	3.47	53.38
	B^{IV}(1B,3Si)	−0.17	18.48
$x = 10$	B^{IIIa}	12.47	32.70
	B^{IIIs}	3.64	54.98
	B^{IV}(1B,3Si)	−0.04	12.32

increasing x. The appeared band of 722 cm^{-1} is attributed to stretching vibrations of Al–O bond in [AlO_4] tetrahedral[18] and the bending vibration of the B–O–B bonds in the borate network;[18,19] the band located around 500 cm^{-1} and 467 cm^{-1} are attributed to the Al–O stretching vibrations in [AlO_6] octahedral and the bending vibration of Si–O–Si.[19,20] Their relative areas are depicted in Fig. 3(b). The results show that the bending vibration of Si–O–Si weakens and the Al–O stretching vibrations increase.

3.3 MAS-NMR spectroscopy

The ^{11}B MAS-NMR spectra of the glasses with different Al_2O_3 content are shown in Fig. 4(a). The spectra show relatively broad peaks located at 11 ppm and 4 ppm are corresponding to asymmetric (B^{IIIa}, boron with 1 or 2 bridging oxygens) and symmetric trigonal (B^{IIIs}, boron with 0 or 3 bridging oxygens) boron units,[21] respectively. The units are showed in the Fig. 5(d), the ball-and-stick models for species in glasses. And another sharper peak centered 0 ppm associated with tetrahedral (BO_4, B^{IV}) boron species,[21] which is similar to borosilicate mineral superstructures danburite units [$B(OB)(OSi)_3$].[22] It is noteworthy that the intensity of [BO_3] units increases distinctly with the increasing of x, indicating the rising amount of [BO_3] units in glasses. In order to quantitatively figure out the distribution of B^{III} and B^{IV} units of boron in glasses, the ^{11}B MAS-NMR spectra were deconvoluted and the example of $x = 5$ was showed in Fig. 5(a), and their NMR parameters, the isotropic chemical shift (δ_{iso}) and the relative amount of structure units, were showed in Table 1. The δ_{iso} of all boron units shifts to a higher value obviously with the increasing x, *i.e.* the value shifts from 11.97 to 12.47 for B^{IIIa}, from 3.17 to 3.64 for B^{IIIs} and from −0.28 to −0.04 for B^{IV}. In addition, the relative amount of B^{IIIa} units increases from 26.44% to 32.7% and B^{IIIs} is from 44.68% to 54.98%, while the B^{IV} units decrease from 28.88% to 12.32% with the increasing of Al_2O_3 content (Table 1). The results are in accordance with previous outcome revealed by the band at 1234 cm^{-1} and 928 cm^{-1} in FT-IR.

Fig. 4(b) revealed the ^{27}Al MAS-NMR spectra of the glasses with $x = 1$, 5 and 10. The spectra showed a narrow peak centered at 55 ppm are associated with Al^{IV} unit[23] and the peak is sharper with the increasing of x, which shows the enhancement of Al units in glasses. In addition, the peaks are asymmetrical and broader demonstrating the presence of higher Al coordination,[23] such as Al^{V} and Al^{VI} units. In order to quantitatively clarify the fractions and distribution of different Al coordination in glasses, the spectral deconvolution was performed using Gaussian by fitting one line shape and an example of $x = 5$ was presented in Fig. 5(b), and the isotropic chemical shift (δ_{iso}) and the relative amount of different Al coordination units were showed in Table 2. The peaks having chemical shifts around 55, 33 and 6.7 ppm can be attributed to Al^{IV}, Al^{V} and Al^{VI} species (as showed in Fig. 5(d)),[13] respectively. With the increasing of x, the relative amount of Al^{IV} units decreases from 61.82% to 57.04% and the Al^{VI} is from 10.85% to 10.08%, while the Al^{V} increases from 27.31% to 32.87%.

The ^{29}Si MAS-NMR spectra for $x = 0$, 5 and 10 were showed in Fig. 4(c). Deconvolution of ^{29}Si spectra was performed using Gaussian to quantitatively analyze the existence form and fractions of Si units. An example of ^{29}Si deconvolution of $x = 5$ is presented in Fig. 5(c) and their NMR parameters are presented in Table 3. The results showed that two peaks around −84 and −90 ppm for all glasses, which are characteristic of the Q^3 and Q^4 structural units of silicon (as showed in Fig. 5(d)), respectively. The chemical shifts of Q^4 structural units shift from −97.01 to −87.79 ppm and Q^3 has no obvious change. Also, the relative amount of Q^4 structural units increases clearly from 5.78% to 37.4%, while the Q^3 decreases from 94.21% to 62.59% for $x = 0$ to $x = 10$.

The previous structural studies (FT-IR, NMR) have shown that B occurs as B^{IIIa}, B^{IIIs} and B^{IV}(1B,3Si) species, Al occurs in 4, 5, and 6-fold coordination (Al^{IV}, Al^{V} and Al^{VI}) and Si presents in Q^3 and Q^4 units in the glasses. This shows the intermediate oxides Al_2O_3 may partly act as glass network former in glasses researched in this paper. The structural changes (Table 1) that the B^{IV} species resolve into symmetric BO_3 species and non-bridging oxygen can be shown as:[13]

Table 2 NMR parameters for ^{27}Al deconvolution

	Aluminum site	δ_{iso} (ppm)	Amount (%)
$x = 1$	Al^{IV}	57.14	61.82
	Al^{V}	33.27	27.31
	Al^{VI}	6.74	10.85
$x = 5$	Al^{IV}	57.16	61.92
	Al^{V}	33.27	27.44
	Al^{VI}	6.74	10.63
$x = 10$	Al^{IV}	55.31	57.04
	Al^{V}	32.67	32.87
	Al^{VI}	6.74	10.08

Table 3 NMR parameters for ^{29}Si deconvolution

	Silicon units	δ_{iso} (ppm)	Amount (%)
$x = 0$	Q^3	−84.47	94.21
	Q^4	−97.01	5.78
$x = 5$	Q^3	−83.67	72.36
	Q^4	−94.03	27.63
$x = 10$	Q^3	−83.06	62.59
	Q^4	−87.79	37.4

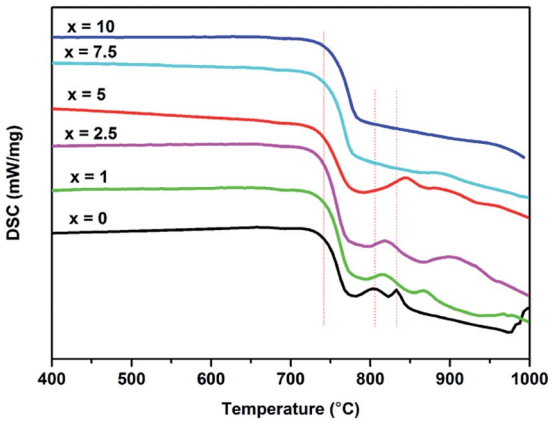

Fig. 6 DSC curve of the studied glasses.

$$BO_4 \leftrightarrow B^{IIIs} + NBO \quad (1)$$

The variation occurred in B^{IIIa} and B^{IIIs} species can be written as the following reaction:[13]

$$B^{IIIs} + NBO \leftrightarrow B^{IIIa} \quad (2)$$

Moreover, the SiO_4 units with n bridging oxygen (Q^n) may combine with the non-bridging oxygen to form the Q^{n-1} unit. The change can be presented as:[13]

$$Q^n + NBO \leftrightarrow Q^{n-1} \quad (3)$$

The shift of Al^{IV}, Al^{V} and Al^{VI} species with NBO can be represented as:

$$Al^{V} \leftrightarrow Al^{IV} + NBO \quad (4)$$

As increasing of Al_2O_3 content, the relative amount of Al^{IV} units decreases while the Al^{V} increases, and the Al^{VI} remains stable (Table 2). These results shows that the Al^{IV} units can capture more NBO to form the Al^{V} units, however, the Al^{IV} units have not enough NBO to shape the Al^{VI} units. The NBOs captured by Al^{IV} units may be originated in the dissociation of BO_4 species (eqn (1)), which was consistent with the result revealed in Table 1. At the same time, due to the competition of Al units to gain the more NBOs, the relative amount of Q^4 structural unit increases while the Q^3 decreases (Table 3). This can account for the eqn (2). Therefore, the increasing concentration of Al substitution in glasses will lead to the decrease of NBOs, which will make the amount of BO_3, Q^4 units increase while BO_4 and Q^3 units decrease.

3.4 Thermal, phase and physical properties of glasses

Fig. 6 presents the DSC plots of all the glasses measured at $\beta = 5$ °C min^{-1}. The curves show 2 crystallization peaks (T_{P1} and T_{P2}), related to the formation of the crystalline phase of wollastonite[24] and borocalcite,[25] respectively. With the increasing of Al_2O_3 content, the T_{P1} and T_{P2} shift in the direction of the higher temperature and gradually disappear. Table 4 presents the values of T_g (glass transition temperature), T_{P1} and T_{P2}. The T_g is obtained from the onset of slope change of the DSC curves. The values of T_g for all glasses don't appear to be much different considering the error factor. The first crystallization peak T_{P1} successively increases with Al_2O_3 content from 805 to 945 °C, however, the second crystallization peak T_{P2} increases obviously with increasing x up to $x = 5$ mol%, and then disappears with the further increasing x in the whole measuring temperatures.

Fig. 7(a) shows the XRD patterns of all glasses isothermally treated once for 1 h at temperature of 850 °C with $x = 0$, 2.5, 7.5 and 10. It could be observed that the peak of crystallization become weaker gradually with the increasing of x, and the glass with $x = 10$ remains the glassy state. The main diffraction peaks for $x = 0$, 2.5 and 7.5 can be indexed to the $CaSiO_3$ (JCPDS No. 10-0487), and a few diffraction peaks corresponding to CaB_2O_4 (JCPDS No. 01-0833) phase. This result conforms to the change of crystallization peaks (T_{P1} and T_{P2}) in DSC analysis as shown in Fig. 6. The Fig. 7(b)–(d) show the XRD patterns of glasses with $x = 0$, 5 and 10, respectively. All samples were isothermally treated four times for 1 h at temperature of 850 °C. Fig. 7(b) revealed that the patterns of sample with $x = 0$ implemented repeated heat treatment were about the same. This result illustrates the sample was crystallized completely when heated at the first time. For sample with $x = 5$, the repeated heat treatment makes the crystallization more complete. However, for sample with $x = 10$, the crystallization was emerged until the third time heat treatment. This observation confirms previous findings, that chemically weak inclusions do not provide active foreign nucleation substrates.[26] One of the most remarkable things about these patterns is that the crystalline phases, not just the $CaSiO_3$ and CaB_2O_4 phase, the most is the Ca_2SiO_4 (JCPDS No. 49-1672). These results revealed that the addition of Al_2O_3 in glasses may hinder the crystallization of CBS glasses. This can be ascribed to the addition of Al_2O_3 dopants, dissolved

Table 4 Characteristic temperatures and physical properties for all glasses

	T_g (°C)	First peak T_{P1} (°C)	Second peak T_{P2} (°C)	ρ (g cm^{-3})	V_m (cm^{-3})	$\rho_{B\ units}$ (g cm^{-3})
$x = 0$	745	805	833	2.845 ± 0.004	26.8	3.18
$x = 1$	744	816	867	2.832 ± 0.004	27.0	—
$x = 2.5$	746	818	902	2.824 ± 0.003	27.3	—
$x = 5$	744	845	955	2.810 ± 0.003	27.6	2.87
$x = 7.5$	747	884	—	2.801 ± 0.004	27.9	—
$x = 10$	750	945	—	2.785 ± 0.003	28.2	2.83

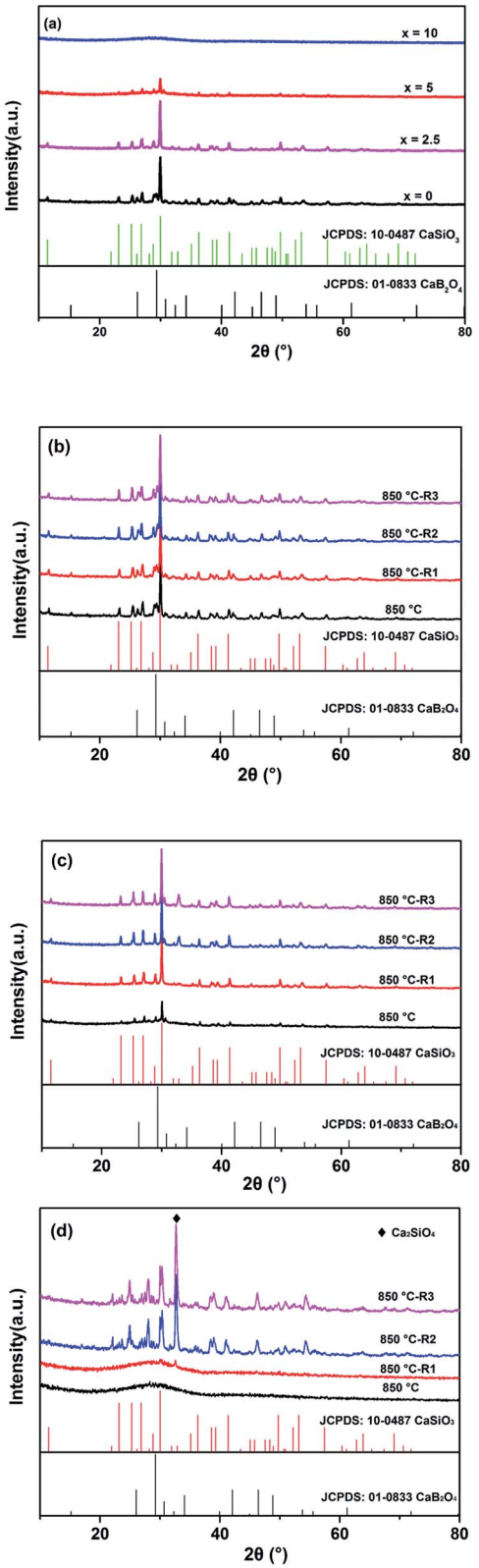

Fig. 7 X-ray diffraction patterns of crystallized glasses at temperature of 850 °C. (a) The patterns glasses isothermally treated one time for $x =$ 0, 2.5, 5 and 10. The patterns of glasses isothermally treated four times (b) $x = 0$; (c) $x = 5$; (d) $x = 10$.

in glass system, modifies the thermodynamic equilibrium of the system and this change is mainly entropy driven and also slowdown the kinetics of crystallization.[27] The addition of Al_2O_3 leads to the reconnection of fractured silicon oxygen tetrahedron and a large extent of atomic rearrangements. This will make the glass need higher thermal energies to crystallize, resulting the increasing of crystallization temperature (Fig. 6 and Table 4).

The density and the molar volume (V_m) of all glasses for $x =$ 0, 1, 2.5, 5, 7.5 and 10 also showed in Table 4. The molar volume (V_m) could be calculated using the following formula:[28]

$$V_m = \frac{M}{\rho} \quad (5)$$

where M and ρ are molecular weight and density of the glass, respectively. As shown in Table 4, the density (ρ) of glasses decreased linearly form 2.845 to 2.786 g cm^{-3} with increasing Al_2O_3 content, while the molar volume (V_m) of the glasses increases linearly. The physical properties of borosilicate glasses depend on the structural units in glasses, which are closely bound up with BO_3, BO_4, Q^n units and Al species. Based on the deconvolution results in FT-IR, the relative areas of the peak corresponding to 722 cm^{-1} in sample with $x = 0$ were 3.53%, while the relative areas of the peaks corresponding to 722 cm^{-1} and 500 cm^{-1} in sample with $x = 10$ were 4.94% and 3.27%, respectively. Therefore, the relative areas of Al–O in sample with $x = 10$ were approximately 4.5%, and the relative areas of B–O and Si–O were 48% and 46%, respectively. So, the Al species make up only a small percentage in glass system. In addition, the Al species changed a little (showed in Table 2), both of which cause a small contribution to the change of density. The change (Q^4 units increase Q^3 units decrease) occurred in Q^n units will make the density increase. The impacts of B units on the density of glasses can be calculated according to eqn (6):

$$\rho = \frac{w_1\% + w_2\% + w_3\%}{w_1\%/\rho_1 + w_2\%/\rho_2 + w_3\%/\rho_3} \quad (6)$$

where w and ρ are the percentage and density of B^{IIIa}, B^{IIIs} and B^{IV} units, respectively. The value of w_1, w_2 and w_3 was showed in Table 1. The density of the symmetric BO_3 unit is ~1.87 g cm^{-3}, for the BO_4 tetrahedron ~6.77 g cm^{-3} and for the asymmetric BO_3 unit ~8.10 g cm^{-3}.[29] The densities of B units for samples with $x = 0$, 5 and 10 were calculated and was listed in Table 4 based on the eqn (6). It can be seen that the $\rho_{B\ units}$ decreases with the increasing of x value, and its influence outweighs the Q^n units. These factors make the density of glasses decrease with the increasing Al_2O_3 content.

4. Conclusions

The current study using NMR, FT-IR, DSC and XRD investigated the role of Al on structure and crystallization of CBS glass when added at a small concentration. The Al partly plays the network former role in CBS glasses and the Al goes into the glass network in 4-fold, 5-fold and 6-fold coordination whereas B goes in as both 4- and 3-fold coordination. The Si occurred in the form Q^3

and Q^4 units. With the increasing of Al_2O_3 content, the amount of BO_3, Q^4 units increase while BO_4, Q^3 units decrease. This is due to the NBOs competition occurred in Al, B and Si units. The density (ρ) of glasses decreased linearly with increasing Al_2O_3 content, while the molar volume (V_m) of the glasses increases linearly. The glass transition temperatures for all glasses don't appear to be much different, while the crystallization peaks of glasses containing Al shift to higher temperatures and disappear. At the same time, the peaks of crystallization become weaker gradually with the increasing of x. These results indicate that Al can hinder the crystallization of CBS glasses.

Acknowledgements

The authors thank the National Center for Magnetic Resonance in Wuhan acquiring the MAS-NMR measurement. This work was supported by the fund of the Basic Applied Research Foundation of Yunnan Province, China (Grant No. 2016FD125, 2016FB083), the 551 project of Kunming and Science &Technology Program of Yunnan Province (No. 2014DC019).

References

1 G. Shao, X. Wu, Y. Kong, X. Shen, S. Cui, X. Guan, C. Jiao and J. Jiao, *J. Alloys Compd.*, 2016, **663**, 360–370.
2 M. Y. Hassaan, H. M. Osman, H. H. Hassan, A. S. El-Deeb and M. A. Helal, *Ceram. Int.*, 2017, **43**, 1795–1801.
3 M. Klinger-Strobel, O. Makarewicz, M. W. Pletz, A. Stallmach and C. Lautenschlager, *J. Mater. Sci.: Mater. Med.*, 2016, **27**, 175.
4 M. Sitarz, *J. Non-Cryst. Solids*, 2011, **357**, 1603–1608.
5 M. Ma, Z. Liu, F. Zhang, F. Liu, Y. Li and R. Bordia, *J. Am. Ceram. Soc.*, 2016, **99**, 2402–2407.
6 S. Cetinkaya Colak, I. Akyuz and F. Atay, *J. Non-Cryst. Solids*, 2016, **432**, 406–412.
7 S. Khan, G. Kaur and K. Singh, *Ceram. Int.*, 2017, **43**, 722–727.
8 J.-Z. Liu, X.-F. Wu, N.-X. Xu, Q.-L. Zhang and H. Yang, *J. Mater. Sci.: Mater. Electron.*, 2015, **26**, 8899–8903.
9 D. R. Neuville, L. Cormier and D. Massiot, *Chem. Geol.*, 2006, **229**, 173–185.
10 S. Stefanovsky, K. Fox and J. Marra, *MRS Proceedings*, 2013, **1518**, 53–58.
11 A. K. Yadav and P. Singh, *RSC Adv.*, 2015, **5**, 67583–67609.
12 A. Saini, A. Khanna, V. K. Michaelis, S. Kroeker, F. González and D. Hernández, *J. Non-Cryst. Solids*, 2009, **355**, 2323–2332.
13 S. Sen, Z. Xu and J. Stebbins, *J. Non-Cryst. Solids*, 1998, **226**, 29–40.
14 K. Singh, I. Bala and V. Kumar, *Ceram. Int.*, 2009, **35**, 3401–3406.
15 J. Wan, J. Cheng and P. Lu, *J. Wuhan Univ. Technol., Mater. Sci. Ed.*, 2008, **23**, 419–421.
16 A. Winterstein-Beckmann, D. Möncke, D. Palles, E. I. Kamitsos and L. Wondraczek, *J. Non-Cryst. Solids*, 2014, **405**, 196–206.
17 K. Rao, *Structural chemistry of glasses*, Elsevier, 2002.
18 N. Santha, T. Nideep and S. Rejisha, *J. Mater. Sci.: Mater. Electron.*, 2012, **23**, 1435–1441.
19 G. J. Mohini, N. Krishnamacharyulu, G. Sahaya Baskaran, P. V. Rao and N. Veeraiah, *Appl. Surf. Sci.*, 2013, **287**, 46–53.
20 H. Shao, H. Q. Zhou and X. D. Shen, *Adv. Mater. Res.*, 2011, **189–193**, 4466–4471.
21 A. Gaddam, H. R. Fernandes and J. M. F. Ferreira, *RSC Adv.*, 2015, **5**, 41066–41078.
22 B. G. Parkinson, D. Holland, M. E. Smith, A. P. Howes and C. R. Scales, *J. Phys.: Condens. Matter*, 2007, **19**, 415114.
23 S. H. Risbud, R. J. Kirkpatrick, A. P. Taglialavore and B. Montez, *J. Am. Ceram. Soc.*, 1987, **70**, C-10–C-12.
24 J. H. Jean, C. R. Chang and C. D. Lei, *J. Am. Ceram. Soc.*, 2004, **87**, 1244–1249.
25 C. R. Chang and J. H. Jean, *J. Am. Ceram. Soc.*, 1999, **82**, 1725–1732.
26 R. Müller, R. Meszaros, B. Peplinski, S. Reinsch, M. Eberstein, W. A. Schiller and J. Deubener, *J. Am. Ceram. Soc.*, 2009, **92**, 1703–1708.
27 A. Gaddam, H. R. Fernandes, M. J. Pascual, J. M. F. Ferreira and L. Pinckney, *J. Am. Ceram. Soc.*, 2016, **99**, 833–840.
28 A. Gaddam, H. R. Fernandes and J. M. Ferreira, *RSC Adv.*, 2015, **5**, 41066–41078.
29 H. Doweidar, K. El-Igili and S. A. El-Maksoud, *J. Phys. D: Appl. Phys.*, 2000, **33**, 2532.